Current THD Analysis in Direct Model Predictive Control

Baljit Riar*, Tobias Geyer† and Regan Zane*
*Department of Electrical and Computer Engineering
Utah State University, USA
† ABB Corporate Research, Baden-Dättwil, Switzerland
Emails: baljit.riar@usu.edu, t.geyer@ieee.org, and regan.zane@usu.edu

***Abstract*—Direct model predictive control (MPDxC) appears to be a strong candidate for high-power applications, because it can achieve very low switching frequencies and keep variables of concern, such as power, current, torque and flux, within specified bounds. The width of bounds is observed to regulate THD of a current when MPDxC is used for controlling the current. This paper describes mathematically the linear relationship in between THD and width of the current bounds and, therefore, evaluates THD without running detailed and time consuming simulations. This mathematical function is valid over a range of bound widths for which the current ripple is approximated to be a piecewise linear function. In the case of a three phase system, the function specifies the upper bound of the THD values, whereas an optimized pulse patterns (OPP) specifies the lower bounds of the THD values. The feasibility of the function over a range of bound widths is demonstrated through simulations and experimental results of a 830-VA single phase converter, and simulations of a 6.78-MVA grid-connected three phase converter.**

***Index Terms*—Current control, direct model predictive control, total harmonic distortion.**

I. Introduction

Historically, model predictive control (MPC) was used in the petrochemical industry for several decades [1]. MPC has been used on an upper supervisory layer in the control hierarchy, where this layer both coordinates and chooses appropriate set-points for lower-layer and fast loops, which are typically proportional-integral (PI) loops. Because of this, long sampling intervals for MPC could be tolerated. The development of fast processors, however, has reduced the computational time of MPC algorithms. Consequently, MPC is used in several applications such as petrochemical, automotive and aerospace industries, and recently in power electronics applications [2]–[4]. Some of the advantages of MPC are simple design, ease of handling constraints, robustness, ease of modeling, and compensation of both system nonlinearities and time delays.

Several formulations of MPC have emerged within the field of power electronics [5]; finite control set (FCS)-MPC, which inherits the above mentioned advantages of MPC, has become popular for both grid- and machine-side converters [5], [6]. FCS-MPC directly manipulates the switch positions of a converter, thus combines the control and modulation problems into a single task. Direct MPC (MPDxC) scheme has emerged in parallel to FCS-MPC to regulate output variables within a set of bounds, and employs an extrapolation strategy to achieve very long prediction horizons [7], [8]. The letter x in MPDxC defines the control of current, torque or power. MPDxC is a strong candidate for controlling high-power converters, because very low switching frequencies can be achieved, thus minimizing the switching losses [2], [9]–[11].

With a model predictive direct current control (MPDCC), it has been observed that total harmonic distortion (THD) of a load current is a linear function of the width of the current bounds. Therefore, THD can be reduced by reducing the bound width. In the case of AC machines, some of the benefits of lower THD values are reduced iron and copper losses in the machine. If MPDCC or a similar scheme is to be used, it is beneficial to predict the THD in the early stages of the converter design, especially, while designing filters. This paper presents a mathematical function to estimate current THD for a given bound width. The estimated values can then be used to select appropriate bounds and to carry out detailed simulations. The accuracy of the proposed function is verified using simulations of a single-phase H-bridge inverter, and experiments of a modular multilevel converter.

With a three phase system, current trajectories cannot be expected to fully utilize the bounds, reducing the width of the bounds. Therefore the values calculated using the function are higher than that of the actual

978-1-5090-5326-1/17/$31.00 ©2017 IEEE

system. At a given switching frequency, an OPP gives the lowest possible THD values. Simulations of 6.78 MVA grid connected system also demonstrate that the actual THD values are upper and lower bounded by the values given by the function and OPP. Comparisons of the waveforms, over a range of operating points, indicate that the function offers a level of accuracy which is similar to simulations and experimental results.

II. Overview of Model Predictive Direct Current Control

For a typical MPDCC, the behaviour of the variables of concern is predicted over a number of time-steps, the length of which is referred to as the prediction horizon, N_p. The controller then determines a suitable control input over the length of N_p while fulfilling objectives and constraints of the converter. To visualise the concept of MPDCC, consider a converter with three possible switch positions, u_1, u_2 and u_3, shown in Fig. 1. The control objective is to find a suitable switch position that can keep the load current, i_o, within its reference bounds, [-δ δ]. In Fig. 1, the actual trajectory of the current is shown as a thick-solid line, whereas predicted trajectories are shown as thin solid lines, for all three switch positions. At time-step k, the trajectories that can be kept within specified bounds are extrapolated (dashed lines) until they violate the bounds. The extrapolation yields horizons that are significantly longer than one sampling period. A cost function is evaluated over the length of the prediction horizon, and the switch position with the minimum cost is applied to the converter. Here the cost function is application specific and is a measure of the chosen performance indicators such as switching frequency, switching losses, voltage variations etc. At the next sampling instant $k+1$, the control problem is solved again with the new set of measurements giving a new optimal sequence of control inputs, and the process is repeated at the subsequent steps. This method of computing the control law is referred to as the receding horizon policy. Moreover, the MPDCC controller sets the converter switch positions without a modulator, and therefore delays associated with the modulator are avoided, resulting in an improved transient response of the converter. Only a brief overview of the MPDCC concept is given here, because it has been explained in a number of publications, such as [8], [10].

III. Converter Setup

The relationship between THD and bound width is derived for a single-phase inverter, shown in Fig. 2. The inverter when connected to an active load, synthesises

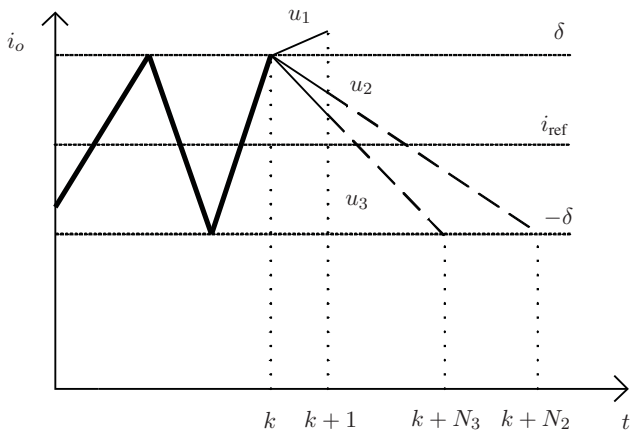

Fig. 1. Current predictions for various switch positions.

an output voltage waveform with three voltage levels and a load current waveform with a ripple, as shown in Fig. 3(a). Although the load current ripple is bounded, the ripple is nonlinear, shown in Fig. 3(b), but it can be approximated as a piecewise linear function for a small bound width or for a large load inductance.

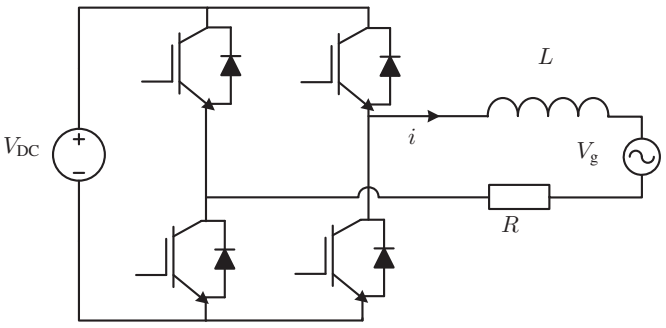

Fig. 2. Single-phase H-bridge inverter.

IV. Total Harmonic Distortion

As shown in Fig. 3(a), ripples in the waveform of the load current is due to steps in the output voltage. The current, therefore, contains harmonics at various frequencies along with the fundamental frequency component and these harmonics do not contribute in transferring energy to the load. These harmonic components, however, account for the THD of the current and can be calculated by using a Fourier series or Parseval's theorem. The load current waveform, $i(t)$, can be expressed as

$$i(t) = \sum_{h=1}^{\infty} i_h(t) = \sum_{h=1}^{\infty} \sqrt{2} I_h cos(\omega_h t + \phi_h) \qquad (1)$$

where h is the harmonic order, I_h and ω_h are the RMS value and angular frequency of the h^{th} harmonic

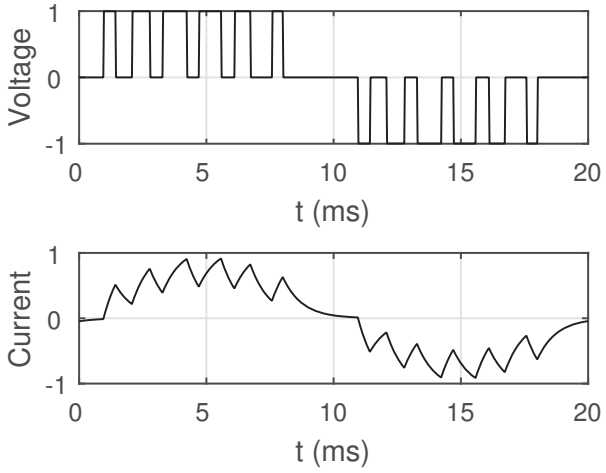

(a)

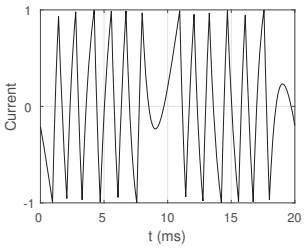

(b)

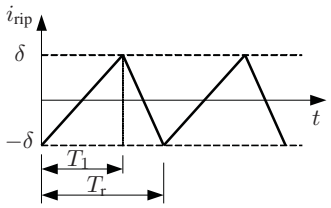

(c)

Fig. 3. (a) Converter output voltage and current waveforms, (b) nonlinear load current ripple, and (c) piecewise linear load current ripple.

current, respectively, and ϕ_h is the angular displacement in between phase voltage and current. The load current ripple, $i_{\text{rip}}(t)$, can then be determined by subtracting the fundamental component, $i_1(t)$, from the load current, $i(t)$. The ripple is approximated to be piecewise linear, and its waveform is shown in Fig. 3(c), where 2δ is the width of the current bounds and T_{r} is the time period of the repetitive ripple waveform.

With the current ripple given by

$$i_{\text{rip}}(t) = \begin{cases} f_1(t) = \frac{2t\delta}{T_1} - \delta, & 0 \le t < T_1 \\ f_2(t) = \frac{-2t\delta}{T_r - T_1} + \frac{\delta(T_r+T_1)}{T_r-T_1}, & T_1 \le t \le T_r \end{cases}, \tag{2}$$

the RMS magnitude of the ripple current can be calculated as

$$\text{RMS}_{i_{\text{rip}}} = \sqrt{\frac{1}{T_r}\left(\int_0^{T_1} f_1(t)^2 \text{d}t + \int_{T_1}^{T_r} f_2(t)^2 \text{d}t \right)}, \tag{3}$$

and after solving the above equation, the expression for the RMS magnitude reduces to

$$\text{RMS}_{i_{\text{rip}}} = \frac{\delta}{\sqrt{3}}. \tag{4}$$

The above expression shows that power or RMS of the ripple current is only defined by the magnitude of the bound width and is independent of the choices of T_1 and T_r. THD of the load current is given by

$$\text{THD}_i = \frac{i_{\text{rip}_{\text{RMS}}}}{I_1} = \frac{\delta}{\sqrt{3} I_1} \tag{5}$$

where I_1 is the RMS value of the fundamental component of the load current. It is evident from (5) that THD of the load current is a linear function of the bound width. Although the level of THD can be affected by under-utilization of the bounds, the MPDCC algorithm usually selects switch positions with which the bounds are well utilized.

V. Results

A. Results: Single-Phase System

Matlab/SIMULINK simulations were carried out to evaluate the load current THD for a range of bound widths and to demonstrate the validity of the mathematical function. The parameters of a single phase system are summarised in Table I. The MPDCC scheme was used to keep the load current within specified bounds while reducing the number of switching transitions. Sampling time with the simulations was 25 μs.

With this scheme, the load current was predicted at time-step $k+1$, for all possible switch positions, $u_j, j \in \{1, 2, 3\}$, i.e. three positions that correspond to an output voltage of V_{DC}, 0 and $-V_{\text{DC}}$, respectively. In the next step, the positions that were predicted to keep future current trajectories within specified bounds were determined and such trajectories were linearly extrapolated from time-step $k+1$ onwards until they collided with the predefined band. This extrapolation gives the length of the prediction horizon, N_j, which was represented in multiples of the sampling interval, T_s. Next, the switch position with the minimum cost (6) was determined and applied at time-step k.

$$C_j = \frac{||u_j(k) - u(k-1)||_1}{N_j}, \quad j \in \{1, 2, 3\} \tag{6}$$

The cost function minimizes the number of switching transitions and, therefore, minimizes the average switching frequency. A receding horizon policy was implemented by repeating these steps at the next sampling instant. Further implementation details related to the control algorithm can be found in [8], [10].

The simulated waveform of the load current, shown in Fig. 4, demonstrates that the current has been regulated within its bounds. All switching transitions appear to take place near the specified bounds.

TABLE I
SYSTEM PARAMETERS FOR MMC AND H-BRIDGE CONVERTER.

Parameter		H-bridge Value	MMC Value
Output frequency	f	50 Hz	50 Hz
Supply voltage	V_{DC}	400 V	400 V
Load RMS current	I	4.5 A	4.5 A
Load resistance	R	0.1 Ω	40 Ω
Load inductance	L	30 mH	30 mH
Arm inductance	l	-	1.2 mH
Module capacitance	C	-	1.72 mF
Grid RMS voltage	V_g	230 V	-

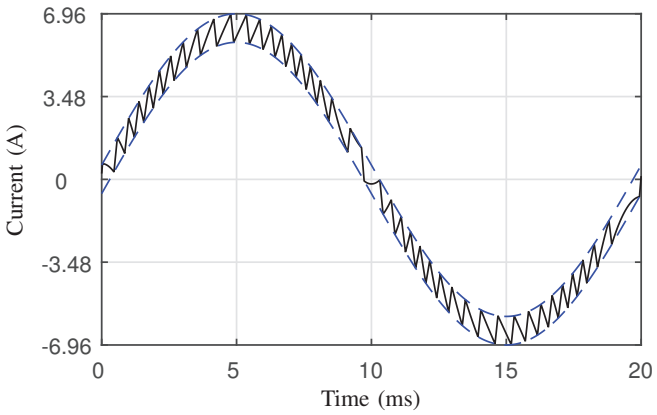

Fig. 4. Simulated waveforms of the load current.

Because the switching frequency with the MPDCC is variable, harmonic frequencies cannot be expected to have only integer multiples of the fundamental frequency, where latter is the case with PWM converters. Therefore, contribution of all the harmonic components is required in order to compute the correct THD values. A Matlab script was used to account for all the harmonics and the values are presented in the following paragraphs.

Fig. 5 shows the THD of the load current for a range of bound widths. Theoretical THD values were calculated using (5). With the sampling time of 25 μs, MPDCC prevents the trajectories from violating the bounds, but results in underutilized bounds or decreased effective bound width. Consequently, simulated THD values are lower than the theoretical values in Fig. 5. Next the sampling time was reduced to 1 μs, achieving a granular control over load current trajectories. With the reduced sampling time, both the simulated and theoretical results closely match each other.

Switching frequency is also plotted over the same range of bound widths, shown in Fig. 6. Here, the frequency was calculated by taking an average of the number of switching transitions over a time period of 100 ms. For lower bound widths, MPDCC with 25 μs

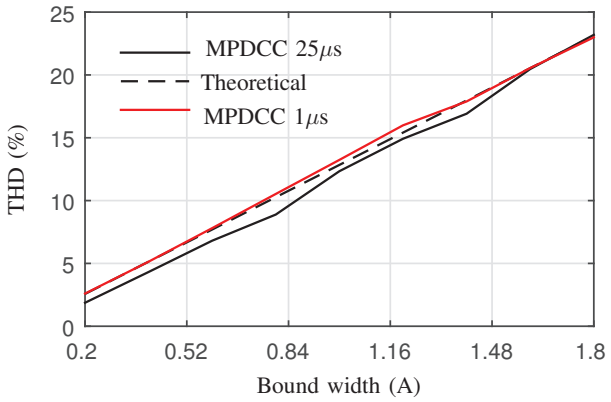

Fig. 5. Simulated THD of the load current against the bound width, δ, with a single-phase H-bridge converter.

of sampling time resulted in the highest switching frequency, because the number of switching transitions are increased to keep the trajectories within the bounds. Sampling time of 1 μs improves utilization of bounds or increases effective bound width and, therefore, resulted in the lowest number of transitions or switching frequency. The frequency is least effected as the bound width increases, where both the waveforms converge to common values.

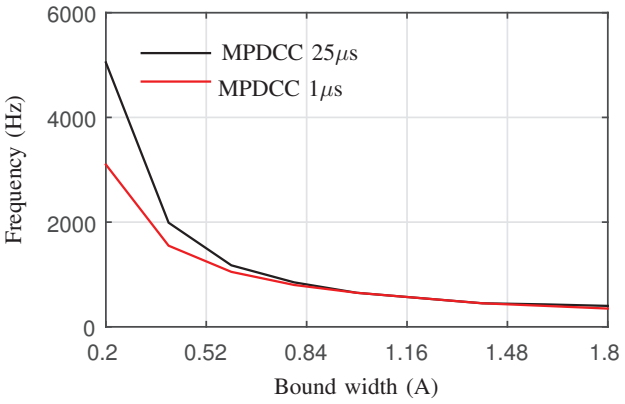

Fig. 6. Simulated switching frequency against the bound width, δ, with a single-phase H-bridge converter

Experimental results of a single-phase modular multilevel converter (MMC) were also used to analyze the effectiveness of the THD function. The MMC setup is shown in Fig. 7 but its algorithm is presented in [10]. With an MMC, THD values for a range of bound widths are shown in Fig. 8. Although simulated results closely match the experiments, there is a discrepancy in the experimental and theoretical results. With the MMC, both a higher sampling time of 125 μs and need for capacitor voltage balancing, as discussed in [10], reduces the effective bound width and, therefore,

theoretical values are higher than both the simulations and experiments. Switching frequency as shown in Fig. 9 decreases with the increasing bound width.

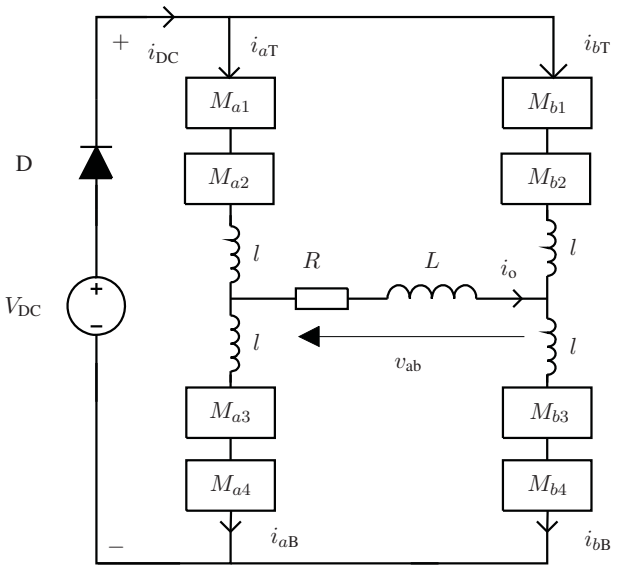

Fig. 7. Experimental setup of the MMC.

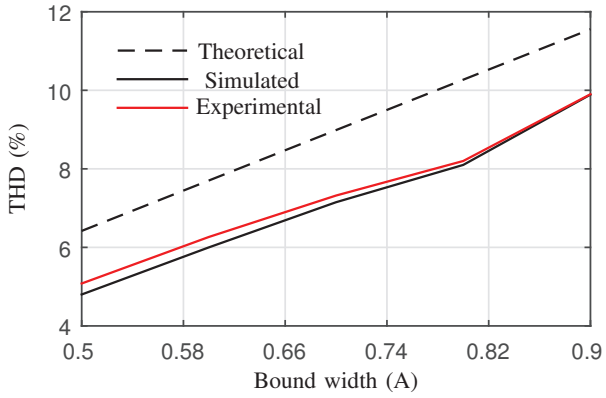

Fig. 8. Experimental THD of the load current against the bound width, δ, with an MMC converter.

Over the range, the THD is a linear function of the bound width, and similarity in between theoretical and simulated results demonstrates the viability of the derived function. It is evident from Figs. 5, 6, 8 and 9 that the THD can be lowered by reducing the bound width, but at the expense of an increased switching frequency.

B. Results: Three-Phase System

In order to demonstrate that the function can also be used for a three phase system, results of a medium-voltage grid-connected neutral point clamped (NPC)

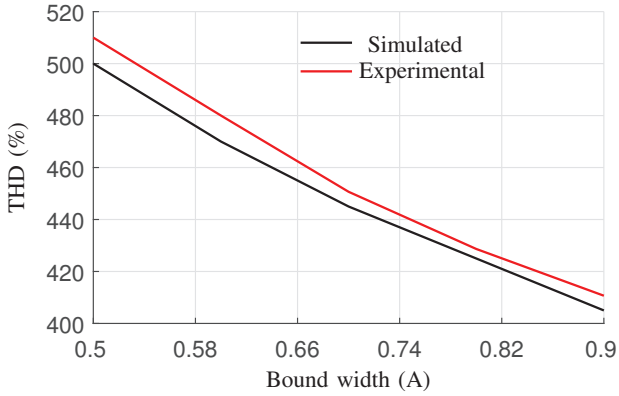

Fig. 9. Experimental switching frequency against the bound width, δ, with an MMC converter.

converter shown in Fig. 10 are presented next, and the system parameters are provided in Table II. In Fig. 10 the inductor, L, corresponds to the line filter inductance, and the voltage, e_r, $r \in \{a, b, c\}$, corresponds to the grid voltage. The MPDCC strategy is implemented according to that outlined in [12]. The sampling time is T_s = 25 μs. It should be noted that the simulation results ignore the non-ideal behavior, such as measurement delay, controller delay, and model mismatch. There are two independent currents with a star connection of the load, and therefore all the three currents cannot be expected to utilize the current bounds at all times. This results in reduction of the bound width, or the effective bound width can now be considered as $\sigma\delta$, where σ is a scaling factor accounting for the under utilized bounds.

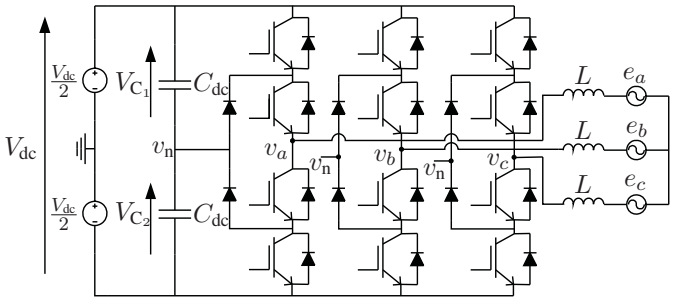

Fig. 10. Schematic of a neutral-point-clamped converter.

Offline calculated optimized pulse patterns (OPP) as described in [13], [14] were also used to evaluate harmonic distortion for a given switching frequency. With the OPP, a quarter wave symmetry is imposed and a number of switching angles that corresponds to the switching frequency are selected. An objective function minimizing the current THD was solved to determine these angles with the converter operating at its rated power (P = 1 p.u. and Q = 0 p.u.). The selected number

TABLE II
RATINGS AND PARAMETERS OF THE MV GRID-CONNECTED CONVERTER USED IN SIMULATIONS.

Ratings and parameters		
Quantity	MV value	p.u. value
DC-link voltage	5 kV	2.041
Grid voltage (V_{rat})	3 kV	1.225
Grid current (I_{rat})	1.29 kA	0.707
Grid apparent power	6.72 MVA	1.000
Grid frequency (f_{rat})	50 Hz	1.000
DC-link capacitance	10 mF	4.200
Grid Inductance	1.13 mH	0.266
Grid Resistance	20 mΩ	0.015

of angles were 2, 3, 5, and 8 such that the switching frequency is an integer multiple of the fundamental frequency.

As shown before, the bound width sets the level of THD and switching frequency of the converter. The simulated THD of the NPC converter is plotted against switching frequency in Fig. 11, demonstrating that the THD decreases with the increasing switching frequency. This reduction in the THD values corresponds to smaller bound widths. Although the derived THD function does not depend on the switching frequency, it is assumed that for a given bound width the switching frequency with the theoretical case is same as the simulations. Theoretical THD values are then plotted against the same switching frequency in Fig. 11. The theoretical values show a trend similar to the simulations, but, as expected, these values are higher than the simulations. The results with the OPP are plotted for switching frequencies of 100, 150, 250 and 400 Hz, where the OPP achieves the lowest possible THD at each frequency.

In addition, simulations were carried out for a two-level (H-bridge) three-phase converter for the parameters

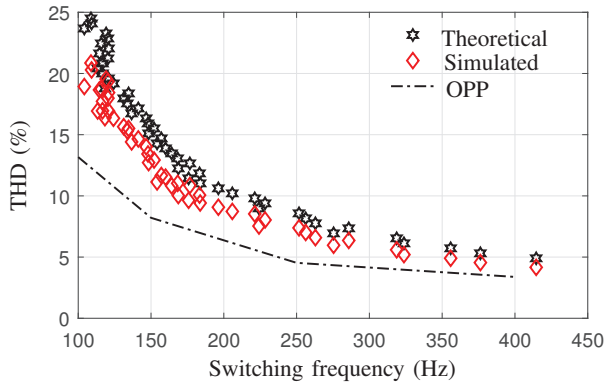

Fig. 11. Simulated THD of the load current against the switching frequency for a three-phase NPC converter.

presented in Table II, and results in Fig. 12 also show the same trend as seen with the NPC converter. Because of two levels in the output voltage waveform, the THD values with the two-level converter are higher than that with the three-level converter.

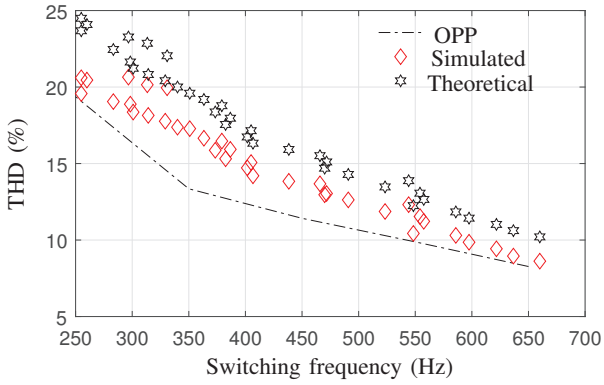

Fig. 12. Simulated THD of the load current against the switching frequency for a three-phase two-level converter.

These results clearly demonstrate that the simulated or actual THD values are bounded by the values with the OPP and theoretical function. Both the THD function and OPP can then be used to predict the level of expected THD in a real system.

VI. CONCLUSIONS

A mathematical function of the load current THD has been presented to reveal that the THD is a linear function of the current bounds. To validate the feasibility of the function, simulated performance of a single-phase inverter has been presented with discussion. Experimental results of a single phase MMC also reveal a linear relationship in between THD and current bounds. An effective bound width or utilization of the bounds increases by decreasing the sampling time, and consequently, simulated results closely match to that predicted by the THD function. Because current trajectories do not fully utilize the bounds with a three-phase system, the actual THD values are upper and lower bounded by the THD function and OPP values. The THD can be lowered by decreasing the bound width, but at the expense of increased switching frequency.

REFERENCES

[1] S. J. Qin and T. A. Badgwell, "A survey of industrial model predictive control technology," *Contr. Eng. Practice*, vol. 11, no. 7, pp. 733–764, Jul. 2003.

[2] T. Geyer, "Low complexity model predictive control in power electronics and power systems," Ph.D. dissertation, Autom. Control Lab. ETH Zurich, 2005.

[3] J. Rodríguez, J. Pontt, C. A. Silva, P. Correa, P. Lezana, P. Cortés, and U. Ammann, "Predictive current control of a voltage source inverter," *IEEE Trans. Ind. Electron.*, vol. 54, no. 1, pp. 495–503, Feb. 2007.

[4] P. Cortés, M. P. Kazmierkowski, R. M. Kennel, D. E. Quevedo, and J. Rodríguez, "Predictive control in power electronics and drives," *IEEE Trans. Ind. Electron.*, vol. 55, no. 12, pp. 4312–4324, Dec. 2008.

[5] J. Rodriguez, M. Kazmierkowski, J. Espinoza, P. Zanchetta, H. Abu-Rub, H. Young, and C. Rojas, "State of the Art of Finite Control Set Model Predictive Control in Power Electronics," *IEEE Transactions on Industrial Informatics*, vol. 9, no. 2, pp. 1003–1016, May 2013.

[6] S. Kouro, P. Cortes, R. Vargas, U. Ammann, and J. Rodriguez, "Model Predictive Control - A Simple and Powerful Method to Control Power Converters," *IEEE Transactions on Industrial Electronics*, vol. 56, no. 6, pp. 1826–1838, Jun. 2009.

[7] T. Geyer, G. Papafotiou, and M. Morari, "Model Predictive Direct Torque Control – Part I: Concept, Algorithm and Analysis," *IEEE Trans. Ind. Electron.*, vol. 56, no. 6, pp. 1894–1905, Jun. 2009.

[8] T. Geyer, "Model Predictive Direct Current Control: Formulation of the Stator Current Bounds and the Concept of the Switching Horizon," *IEEE Ind. Appl. Mag.*, vol. 18, no. 2, pp. 47–59, Mar. 2012.

[9] ——, "A comparison of control and modulation schemes for medium-voltage drives: Emerging predictive control concepts versus PWM-based schemes," *IEEE Trans. Ind. Appl.*, vol. 47, no. 3, pp. 1380–1389, May/Jun. 2011.

[10] B. S. Riar, T. Geyer, and U. K. Madawala, "Model predictive direct current control of modular multilevel converters: Modeling, analysis, and experimental evaluation," *IEEE Transactions on Power Electronics*, vol. 30, no. 1, pp. 431–439, Jan. 2015.

[11] ——, "Model Predictive Direct Current Control of Modular Multi-level Converters," in *Proc. IEEE Int. Conf. Ind. Technol.*, 2013, pp. 582–587.

[12] J. Scoltock, T. Geyer, and U. Madawala, "Model predictive direct current control for a grid-connected converter: LCL-filter versus L-filter," in *Industrial Technology (ICIT), 2013 IEEE International Conference on*, 2013, pp. 576–581.

[13] T. Geyer, N. Oikonomou, G. Papafotiou, and F. D. Kieferndorf, "Model predictive pulse pattern control," *IEEE Transactions on Industry Applications*, vol. 48, no. 2, pp. 663–676, Mar. 2012.

[14] A. Rathore, J. Holtz, and T. Boller, "Synchronous optimal pulsewidth modulation for low-switching-frequency control of medium-voltage multilevel inverters," *IEEE Trans. Ind. Electron.*, vol. 57, no. 7, pp. 2374–2381, Jul. 2010.